The Journal of Neuroscience, February 15, 2002, 22(4):1290–1302

I_h Channels Contribute to the Different Functional Properties of Identified Dopaminergic Subpopulations in the Midbrain

Henrike Neuhoff,* Axel Neu,* Birgit Liss, and Jochen Roeper

Medical Research Council, Anatomical Neuropharmacology Unit, Department of Pharmacology, Oxford University, OX1 3TH United Kingdom

Dopaminergic (DA) midbrain neurons in the substantia nigra (SN) and ventral tegmental area (VTA) are involved in various brain functions such as voluntary movement and reward and are targets in disorders such as Parkinson's disease and schizophrenia. To study the functional properties of identified DA neurons in mouse midbrain slices, we combined patch-clamp recordings with either neurobiotin cell-filling and triple labeling confocal immunohistochemistry, or single-cell RT-PCR. We discriminated four DA subpopulations based on anatomical and neurochemical differences: two calbindin D_{28}-k (CB)-expressing DA populations in the substantia nigra (SN/CB+) or ventral tegmental area (VTA/CB+), and respectively, two calbindin D_{28}-k negative DA populations (SN/CB−, VTA/CB−). VTA/CB+ DA neurons displayed significantly faster pacemaker frequencies with smaller afterhyperpolarizations compared with other DA neurons. In contrast, all four DA populations possessed significant differences in I_h channel densities and I_h channel-mediated functional properties like sag amplitudes and rebound delays in the following order: SN/CB− → VTA/CB− → SN/CB+ → VTA/CB+. Single-cell RT-multiplex PCR experiments demonstrated that differential calbindin but not calretinin expression is associated with differential I_h channel densities. Only in SN/CB− DA neurons, however, I_h channels were actively involved in pacemaker frequency control. In conclusion, diversity within the DA system is not restricted to distinct axonal projections and differences in synaptic connectivity, but also involves differences in postsynaptic conductances between neurochemically and topographically distinct DA neurons.

Key words: HCN channels; dopamine; calbindin; substantia nigra; ventral tegmental area; pacemaker; Parkinson's disease; confocal immunohistochemistry; single-cell RT-PCR

Dopaminergic midbrain (DA) neurons play an important role in voluntary movement, working memory, and reward (Goldman-Rakic, 1999; Kitai et al., 1999; Spanagel and Weiss, 1999). They are involved in disorders such as schizophrenia, drug addiction, and Parkinson's disease (Dunnet and Bjorklund, 1999; Verhoeff, 1999; Berke and Hyman, 2000; Grace, 2000; Svensson, 2000; Tzschentke, 2001). Dopaminergic neurons are distributed in three partially overlapping nuclei: the retrorubral area (RRA, A8), substantia nigra (SN, A9), and ventral tegmental area (VTA, A10), which correspond to different mesotelencephalic projections (Fallon, 1988; Francois et al., 1999; Bolam et al., 2000; Joel and Weiner, 2000). Substantia nigra neurons mainly target the dorsal striatum (mesostriatal projection) and are involved in motor function, whereas those of the VTA project predominantly to the ventral striatum e.g., nucleus accumbens (mesolimbic projection) and to prefrontal cortex (mesocortical projection) and are associated with limbic and cognitive functions (Swanson, 1982; Oades and Halliday, 1987; Carr and Sesack, 2000b).

Received Aug. 29, 2001; revised Nov. 27, 2001; accepted Nov. 30, 2001.

This work was supported by a Medical Research Council grant to J.R. He holds the Monsanto Senior Research Fellowship at Exeter College, Oxford. B.L. is supported by a Royal Society Dorothy Hodgkin Fellowship and a Todd-Bird Junior Research Fellowship at New College, Oxford. We thank Paul Bolam, Jakob Wolfart, and Alison Robson for critically reading this manuscript.

*H.N. and A.N. contributed equally to this work.

Correspondence should be addressed to Dr. Jochen Roeper, Medical Research Council, Anatomical Neuropharmacology Unit, Oxford University, Mansfield Road, Oxford OX1 3TH, UK. E-mail: jochen.roeper@pharm.ox.ac.uk.

H. Neuhoff's present address: Scientific Services, Morphology, Zentrum für Molekulare Neurobiologie Hamburg, D-20251 Hamburg, Germany.

A. Neu's present address: Institute for Neural Signaltransduction, Zentrum für Molekulare Neurobiologie Hamburg, D-20251 Hamburg, Germany.

In the substantia nigra pars compacta (SNc), a dorsal and a ventral tier of DA neurons have been described that project to different neurochemical compartments in the striatum (Maurin et al., 1999; Haber et al., 2000). In addition, some DA neurons are found in substantia nigra pars reticulata (SNr). Ventral tier SNc and SNr DA neurons that do not express the calcium-binding protein calbindin D_{28}-k (CB−), project to striatal patch compartments and in turn receive innervation from striatal projection neurons in the matrix. Conversely, calbindin-positive (CB+) dorsal tier SNc DA neurons project to the striatal matrix while receiving input from the limbic patch compartment. CB+ and CB− DA neurons have also been described in the VTA but little is known about their axonal targets (Gerfen, 1992a; Hanley and Bolam, 1997; Barrot et al., 2000). The function of calbindin in DA neurons is unknown, but CB+ DA neurons appear to be less vulnerable to degeneration in Parkinson's disease and its animal models (Liang et al., 1996; Damier et al., 1999; Gonzalez-Hernandez and Rodriguez, 2000; Tan et al., 2000).

In contrast to their anatomy, it is unknown whether these neurochemically distinct DA subpopulations possess different functional properties. To date, *in vitro* electrophysiological studies have considered DA midbrain neurons mainly as a single population (Pucak and Grace, 1994; Kitai et al., 1999), which shows low-frequency pacemaker activity, broad action potentials followed by a pronounced afterhyperpolarization, and a pronounced sag component that is mediated by hyperpolarization-activated, cyclic nucleotide-regulated cation (I_h, HCN) (for review, see Santoro and Tibbs, 1999) channels (Sanghera et al., 1984; Grace and Onn, 1989; Lacey et al., 1989;

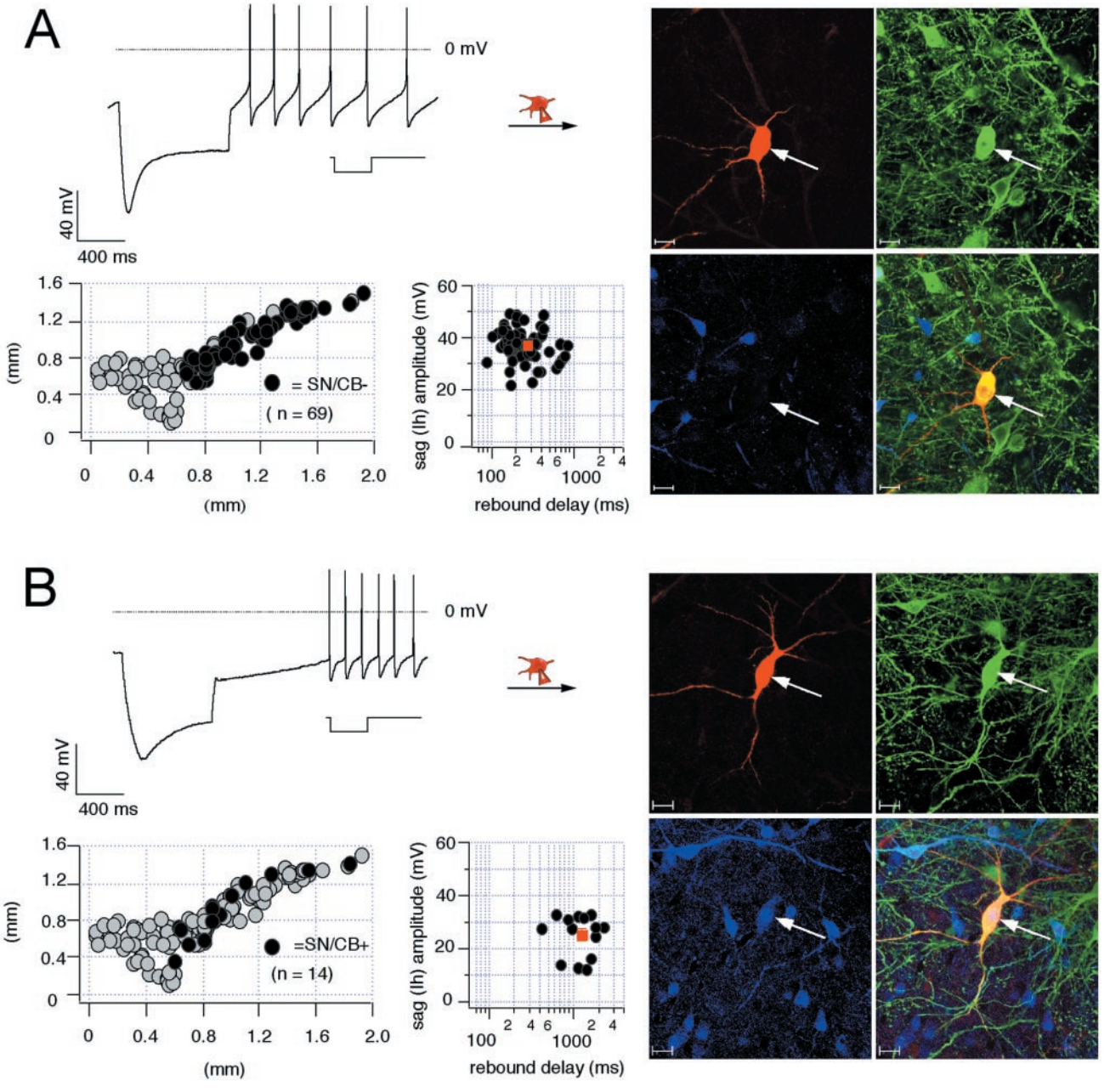

Figure 1. Electrophysiological properties and anatomical distribution of calbindin-positive and calbindin-negative dopaminergic SN neurons. *A,* Current-clamp recording of SN neuron with membrane voltage response to 1 sec injection of hyperpolarizing current (*inset*) to hyperpolarize the cell initially to −120 mV (*left, top panel*). Note the large sag component and the short rebound delay. During recording, the neuron was filled with 0.2% neurobiotin (*filled symbols*, *arrows*). Confocal analysis of coimmunolabeling for neurobiotin (*red, right-top left panel*), TH (*green, right-top right panel*), and CB (*blue, right-bottom left panel*) identified the recorded cell as a dopaminergic (TH+), calbindin-negative SN (SN/CB−) neuron (*overlay, right-bottom right panel*). Scale bars, 20 μm. The anatomical positions of electrophysiologically characterized and immunohistochemically identified SN/CB− neurons ($n = 69$; *black circles*) were plotted in a coronal midbrain map (*left-bottom left panel*) also containing other subpopulations of analyzed DA neurons (*gray circles*). The sag amplitudes of SN/CB− DA neurons were plotted against their corresponding rebound delays (*left-bottom right panel*). The mean sag amplitude and rebound delay were 37.3 ± 0.72 mV and 269.2 ± 19.41 msec, respectively (*red square*). *B,* Current-clamp recording of SN neuron with membrane voltage response elicited as in *A* (*left, top panel*). Note in comparison with *A*, the smaller sag component and prolonged rebound delay. The recorded cell was filled and processed as in *A*. Confocal analysis identified it as a dopaminergic (TH+) calbindin-positive SN (SN/CB+) neuron. The anatomical positions of electrophysiologically characterized and immunohistochemically identified SN/CB+ DA neurons ($n = 14$; *black circles*) were plotted in a coronal midbrain map (*left-bottom left panel*) also containing other subpopulations of analyzed DA neurons (*gray circles*). The sag amplitudes of SN/CB+ neurons were plotted against their corresponding rebound delays (*left-bottom right panel*). The mean sag amplitude and rebound delay were 25.3 ± 2.2 mV and 1262.4 ± 147.5 msec, respectively (Table 1).

Richards et al., 1997). However, *in vivo* studies have highlighted functional differences between subgroups of DA neurons (Wilson et al., 1977; Chiodo et al., 1984; Greenhoff et al., 1988; Shepard and German, 1988; Paladini and Tepper, 1999). Thus, we used a combined electrophysiological, immunohistochemical and molecular approach to investigate the electrophysiological properties of anatomically and neurochemically identified DA neurons.

Table 1. Functional properties of topographically and neurochemically identified SN and VTA DA neurons

DA neurons	Soma size (μm)	Frequency (Hz)	AHP (mV)	AP threshold (mV)	AP amplitude (mV)	Rebound delay (msec)	Pacemaker slope (mV/sec)	I_h sag (mV)
SN/CB− (n = 69)	28.8 ± 0.82	3.3 ± 0.18	−54.7 ± 0.58	−32.0 ± 1.08	55.8 ± 0.91	269.2 ± 19.41	68.7 ± 3.52	37.3 ± 0.72
SN/CB+ (n = 14)	27.6 ± 1.89	2.4 ± 0.265	−56.3 ± 1.51	−33.1 ± 0.99	59.5 ± 2.34	1262 ± 147.5*	22.7 ± 4.63*	25.3 ± 2.18*
VTA/CB− (n = 21)	26.8 ± 1.17	3.6 ± 0.29	−52.8 ± 1.24	−32.7 ± 0.96	55.6 ± 1.91	632.3 ± 101.3*	37.7 ± 1.02*	31.0 ± 1.72*
VTA/CB+ (n = 21)	20.9 ± 1.02*	5.2 ± 0.63*	−45.6 ± 1.68*	−30.5 ± 0.96	49.7 ± 2.12*	1563 ± 82.7*	14.8 ± 0.81*	11.9 ± 1.06*

Asterisks indicate significant differences in comparison with the respective value of the SN/CB− population ($p < 0.0001$; ANOVA).

MATERIALS AND METHODS

Slice preparation, patch-clamp recordings, and data analysis. Coronal midbrain slices were prepared from 12- to 15-d-old C57BL/6J mice as previously described (Liss et al., 1999b) For patch-clamp recordings, midbrain slices were transferred to a chamber continuously perfused at 2–4 ml/min with ACSF containing (in mM): 125 NaCl, 25 $NaHCO_3$, 2.5 KCl, 1.25 NaH_2PO_4, 2 $CaCl_2$, 2 $MgCl_2$, and 25 glucose, bubbled with a mixture of 95% O_2 and 5% CO_2 at room temperature (22–24°C). Patch pipettes (1–2.5 MΩ) pulled from borosilicate glass (GC150TF; Clark, Reading, UK) were filled with internal solution containing (in mM): 120 K-gluconate, 20 KCl, 10 HEPES, 10 EGTA, 2 $MgCl_2$, 2 Na_2ATP, pH 7.3 (290–300 mOsm). For gramicidin-perforated patch-clamp recordings (Akaike, 1999), the patch pipette was tip-filled with internal solution and back-filled with gramicidin-containing internal solution (20–50 μg/ml). For cell filling, at the end of perforated-patch experiments, we converted the configuration to standard whole-cell by gentle suction monitored by changes in capacitive transients in voltage-clamp mode, filled the cell for 2 min, and removed the pipette via the outside-out configuration. Whole-cell recordings were made from neurons visualized by infrared differential interference contrast (IR-DIC) video microscopy with a Newvicon camera (C2400; Hamamatsu, Hamamatsu City, Japan) mounted to an upright microscope (Axioskop FS; Zeiss, Oberkochen, Germany) (Stuart et al., 1993). Recordings were performed in current-clamp and voltage-clamp mode using an EPC-9 patch-clamp amplifier (Heka Elektronik, Lambrecht, Germany). Only voltage-clamp experiments with uncompensated series resistances <10 MΩ were included in the study, and series resistances were electronically compensated (70–85%). The program package PULSE+PULSEFIT (Heka Elektronik, Lambrecht, Germany) was used for data acquisition and analysis. Records were digitized at 2–5 kHz and filtered with low-pass filter Bessel characteristic of 1 kHz cutoff frequency. To compare sag amplitudes of different DA neurons, the amplitudes of the current injections were adjusted in each cell to result in a peak hyperpolarization to −120 mV, and the sag amplitude was determined as repolarization from −120 mV to a steady-state value during the 1 sec current injection. The rebound delay was determined as the time between the end of the hyperpolarizing current injection that initially hyperpolarized the cell to −120 mV and the peak of the first action potential. The pacemaker slope indicates the steepness (in millivolts per millisecond) of the repolarization to threshold. The I_h channel charge transfer (in picocoulombs) was calculated by integrating (nanoampere times milliseconds) the slowly activating inward current component elicited in response to a 2 sec voltage step from −40 to −120 mV. The leak charge transfer (in picocoulombs) was calculated by integrating the time-independent current in response to the same voltage protocol. The I_h channel charge density (picocoulombs per picofarad) was calculated by dividing the I_h channel charge transfer (picocoulomb) by the whole-cell capacitance (picofarad) as a measure of cell size. DMSO or H_2O stock solutions of drugs were diluted 1000-fold in an external solution containing (in mm): 145 NaCl, 2.5 KCl, 10 HEPES, 2 CaCl2, 2 MgCl2, and 25 glucose, pH 7.4, and applied locally under visual control using a buffer pipette attached to a second manipulator. Switching between control and drug-containing solutions was controlled by an automated application system (AutoMate Scientific, Oakland, CA). Data were given as mean ± SEM. Concentration–response data for cesium and ZD7288 were fitted according to the Hill relationship ($I/I_{max} = 1/(1 + [X]/IC_{50})^n$). To evaluate statistical significance, data were subjected to Student's t test (Excel, Microsoft Office) or ANOVA test in StatView (Abacus Concept, Inc. Berkeley, CA).

Immunocytochemistry and confocal microscopy. Slices were fixed with 4% paraformaldehyde in PBS, pH 7.4, for 30 min at room temperature. The fixative was removed with four washes of PBS solution. Slices were treated with 1% Na-borohydride (Sigma, Poole, UK) dissolved in PBS for 10 min and again washed four times in PBS for 5 min. Slices were treated for 20 min with a blocking solution containing 10% horse serum, (Vector Laboratories, Burlingame, CA), 0.2% BSA, and 0.5% Triton X-100 (Sigma) for permeabilization in PBS. The blocking solution was removed with two washes of PBS. Primary antibodies [rabbit anti-tyrosine hydroxylase (1:1000; Calbiochem, San Diego, CA), monoclonal anti-calbindin D-$_{28}$k (1:1000; Swant, Bellinzona, Switzerland)] were applied overnight in a carrier solution consisting of 1% horse serum, 0.2% BSA, and 0.5% Triton X-100 in PBS. Afterward, slices were washed four times in PBS for 5 min and then incubated with the following secondary antibodies: Alexa 488 goat anti-rabbit IgG (1:1000; Molecular Probes, Eugene, OR); avidin-Cy3 (1:1000; Amersham Biosciences, Little Chalfont, UK), and goat anti-mouse-Cy5 (1:1000; Amersham Biosciences) for 90 min at room temperature in 0.5% Triton X-100 in PBS. Subsequently, slices were washed six times in PBS for 5 min and mounted in Vectashield Mounting Medium (Vector Laboratories) to prevent rapid photo bleaching. Slices were analyzed using a Zeiss LSM 510 confocal laser-scanning microscope. Fluorochromes were excited with an argon laser at 488 nm using a BP505–530 emission filter, with a HeNe laser at 543nm in combination with a BP560–615 emission filter, and HeNe laser at 633nm and a LP 650 emission filter. To eliminate any cross-talk, the multitracking configuration was applied. Images were taken at a resolution of 1024 × 1024 pixels with a Plan-Apochromat 40×/1.3 oil phase 3 Zeiss objective using the LSM 510 software 2.5.

Single-cell RT-PCR. Single-cell RT-PCR experiments and controls were performed as previously described (Liss et al., 1999b, 2001). After reverse transcription, the cDNAs for tyrosine hydroxylase (TH), GAD_{67}, calbindin (CB), calretinin (CR), and parvalbumin (PV) were simultaneously amplified in a multiplex PCR using the following set of primers (from 5′ to 3′). Primer pairs for TH, GAD_{67}, and CB were identical to those used in Liss et al. (1999a): calbindin (GenBank accession number M21531) sense: CGCACTCTCAAACTAGCCG (87), antisense: CAGCCTACTTCTTTATAGCGCA (977): calretinin (GenBank accession number cDNA: X739851, gene ABO37964.1) sense: AGAGAGGCTTAAGATCTCCGG (861), antisense: CAGAAGCCTAAATCATACAGCG (4909), parvalbumin (GenBank accession number X59382) sense: AAGTTGCAGGATGTCGATGA (47), antisense: CCTACAGGTGGTGTCCGATT (589). First multiplex PCR was performed as hot start in a final volume of 100 μl containing the 10 μl RT reaction, 100 pmol of each primer, 0.2 mM of each of the four deoxyribonucleotide triphosphates (Amersham Biosciences), 1.8 mM $MgCl_2$, 50 mM KCl, 20 mM Tris-HCl, pH 8.4, and 3.5 U of *Taq*-polymerase (Invitrogen, Gaithersburg, MD) in a PerkinElmer Life Sciences (Emeryville, CA) thermal cycler 480C with the following cycling protocol: after 5 min at 94°C 35 cycles (94°C, 30 sec; 58°C, 60 sec; 72°C 3 min) of PCR were performed followed by a final elongation period of 7 min at 72°C. The nested PCR amplifications were performed in individual reactions, in each case with 2.5 μl of the first PCR-reaction product under similar conditions with the following modifications: 50 pmol of each primer, 2.5 U of *Taq* polymerase, 1.5 mM $MgCl_2$, and a shorter extension time (60 sec) using the following primer pairs: calbindin sense: GAGATCTGGCT-

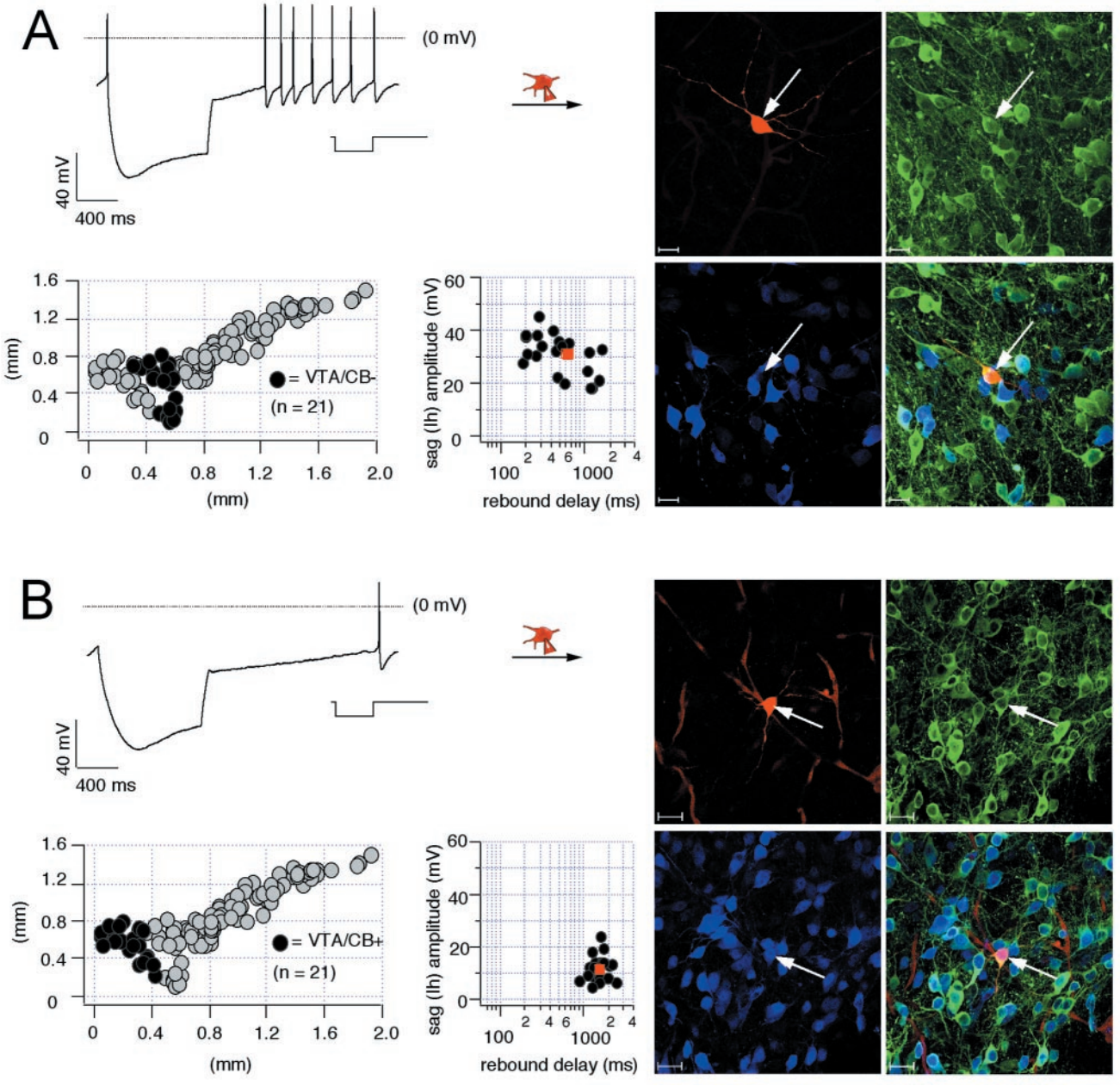

Figure 2. Electrophysiological properties and anatomical distribution of calbindin-positive and calbindin-negative dopaminergic VTA neurons. *A,* Current-clamp recording of VTA neuron with membrane voltage response to 1 sec injection of hyperpolarizing current (*inset*) to hyperpolarize the cell initially to −120 mV (*left, top panel*). During recording, the neuron was filled with 0.2% neurobiotin (*filled symbols, arrows*). Confocal analysis of coimmunolabeling for neurobiotin (*red, right-top left panel*), TH (*green, right-top right panel*), and CB (*blue, right-bottom left panel*) identified the recorded cell as a dopaminergic (TH+), calbindin-negative VTA (VTA/CB−) neuron (*overlay, right-bottom right panel*). Scale bars, 20 μm. The anatomical positions of electrophysiologically characterized and immunohistochemically identified VTA/CB− neurons ($n = 21$; *black circles*) were plotted in a coronal midbrain map (*left-bottom left panel*) also containing other subpopulations of analyzed DA neurons (*gray circles*). The sag amplitudes of VTA/CB− DA neurons were plotted against their corresponding rebound delays (*left-bottom right panel*). The mean sag amplitude and rebound delay were 31.0 ± 1.7 mV and 632.3 ± 101.3 msec, respectively (*red square*). *B,* Current-clamp recording of VTA neuron with membrane voltage response elicited as in *A* (*left, top panel*). In comparison with *A*, note the prolonged rebound delay. The recorded cell was filled and processed as in *A*. Confocal analysis identified it as a dopaminergic (TH+), calbindin-positive (VTA/CB+) neuron (*overlay, right-bottom right panel*). The anatomical positions of electrophysiologically characterized and immunohistochemically identified VTA/CB+ DA neurons ($n = 21$; *black circles*) were plotted in a coronal midbrain map (*left-bottom left panel*) also containing other subpopulations of analyzed DA neurons (*gray circles*). The sag amplitudes of VTA/CB+ neurons were plotted against their corresponding rebound delays (*left-bottom right panel*). The mean sag amplitude and rebound delay were 11.9 ± 1.1 mV and 1262.4 ± 147.5 msec, respectively (Table 1).

TCATTTCGAC (167), antisense: AGTTCCAGCTTTCCGTCATTA (606): calretinin sense: GAAGCACTTTGATGCTGACG (4803), antisense: CATTCTCATCAATATAGCCGCT (414). parvalbumin sense: GACATCAAGAAGGCGATAGGA (87), antisense: CAGAAGAATGGCGTC ATCC (538). To investigate the presence and size of the amplified fragments, 15 μl aliquots of PCR products were separated and visualized in ethidium bromide-stained agarose gels (2%) by electrophoresis. The predicted sizes (in base pairs) of the PCR-generated fragments were: 377 (TH), 702 (GAD_{67}), 440 (calbindin), 580 (calretinin), and 452 (parvalbumin). All individual PCR products were verified by direct sequencing.

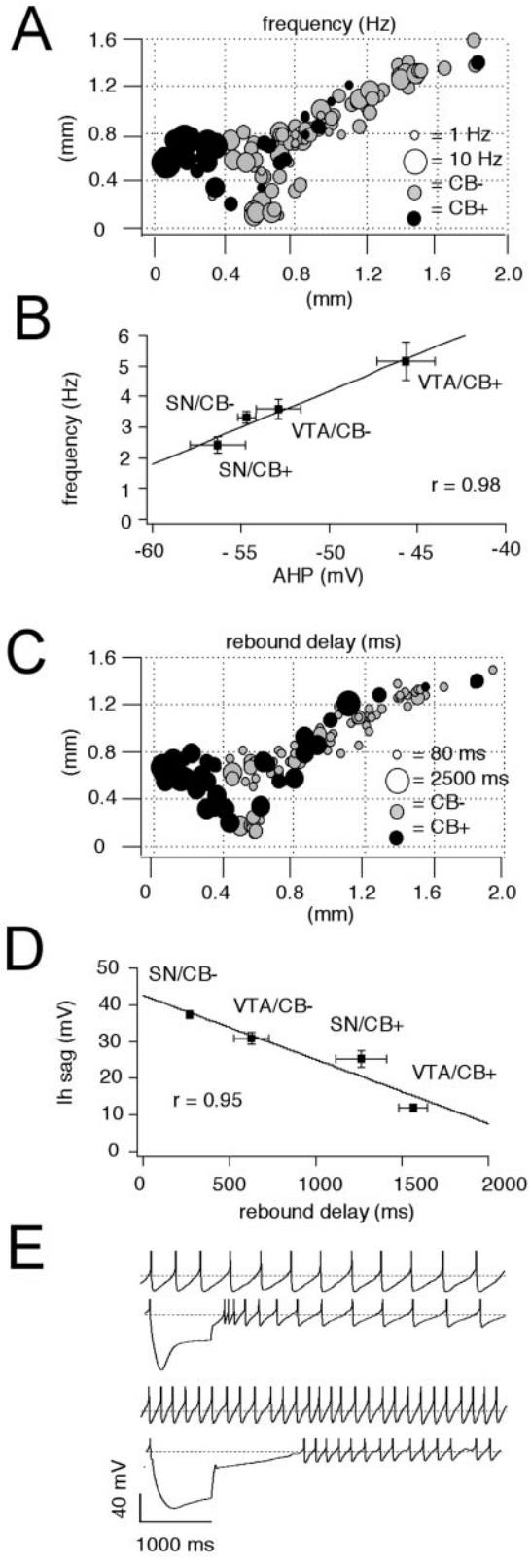

Figure 3. Anatomical distribution of pacemaker frequencies and rebound delays in DA neurons. *A,* Anatomical distribution of spontaneous pacemaker frequencies in immunohistochemically characterized and identified DA neurons ($n = 125$). CB+ neurons are represented by *black circles*, and CB− neurons by *gray circles*. Frequency is coded by symbol size (1–10 Hz). VTA/CB+ neurons display significantly higher frequencies than SN/CB− neurons ($p < 0.0001$) (Table 1). *B,* Linear scaling between mean spike frequencies of different DA subpopulations and respective mean amplitudes of their AHPs ($r = 0.98$). *C,* Anatomical distribution of subthreshold rebound delays in immunohistochemically characterized and identified DA neurons ($n = 125$). CB+ neurons are represented by *black circles*, and CB− neurons by *gray circles*. Delay is coded by symbol size (80–2500 msec). The rebound delays are significantly different between all four DA subpopulations. CB+ neurons possess longer delays compared with CB− neurons in both SN and VTA (Table 1). *D,* Linear scaling between mean rebound delays frequencies of different DA subpopulations and respective mean sag amplitudes ($r = 0.95$). *E,* Current-clamp recordings of spontaneous pacemaker activities and membrane responses to hyperpolarizing current injection of a SN/CB− neuron (*top panels*) in comparison with a VTA/CB+ neuron (*bottom panels*). SN/CB− neurons displayed slower discharge but faster rebound compared with VTA/CB+ neurons. SN/CB− neurons displayed transient postinhibitory excitation, and VTA/CB+ neurons possessed prolonged postinhibitory hypoexcitability.

RESULTS

We studied the electrophysiological properties of >300 identified dopaminergic midbrain neurons combining patch-clamp techniques with either triple-labeling confocal immunohistochemistry or single-cell RT-PCR in midbrain slices of 12- to 15-d-old C57BL/6J mice. In the SNc, calbindin-negative (SN/CB−) DA neurons were most abundant ($n = 69$ of 83; 83%). They displayed an electrophysiological phenotype consisting of large afterhyperpolarizations (AHPs), a very prominent sag during injection of hyperpolarizing current, and a rebound delay of ~200–400 msec (Fig. 1*A*, Table 1). Note also the transient acceleration of spike frequency during repolarization. The anatomical positions of SN/CB− DA neurons are plotted in Figure 1*A,* indicating that they cover the entire extent of the mediolateral axis of the SNc. Also, these neurons are found both on the ventral and dorsal margins of the SNc. Figure 1*A* also shows that sag amplitudes and rebound delays of SN/CB− DA neurons cluster around their respective mean values. We did find a weak correlation of sag amplitudes and rebound delays of SN/CB− DA neurons in respect to their positions on the mediolateral ($r = 0.26$) or dorsoventral ($r = 0.29$) axis of the SN with ventrolateral SN/CB− DA neurons displaying larger sag amplitudes and shorter rebound delays.

The minor population ($n = 14$ of 83; 17%) of calbindin-positive (SN/CB+) DA neurons showed significant differences in their subthreshold behavior with smaller sag amplitudes and ~4.5-fold prolonged rebound delays (Fig. 1*B*, Table 1). There was also no transient acceleration of spike frequency during repolarization in SN/CB+ DA neurons. They were scattered along the entire medial-lateral axis of the SNc with a majority ($n = 9$ of 14; 64%) being positioned at the dorsal margin of the SNc. The functional properties of SN/CB+ DA neurons showed also a weak association with their anatomical position along the mediolateral ($r = 0.34$) or dorsoventral ($r = 0.40$) axis of the SN. Comparison of the scatter plots in Figure 1 demonstrates that there is little overlap between sag amplitudes and rebound delays of SN/CB+ and SN/CB− DA neurons.

In the VTA, CB+ and CB− DA neurons were found in similar abundance (CB+, $n = 21$ of 42, 50%; CB−, $n = 21/42$, 50%) but appeared anatomically segregated. Identified VTA/CB− DA neurons, localized to lateral regions of the VTA, showed electrophysiological properties that were in between those of SN/CB+ and SN/CB− DA neurons (Fig. 2*A*, Table 1). Thus, VTA/CB− DA neurons possessed smaller sag amplitudes and longer rebound delays compared with SN/CB− DA neurons. These electrophysiological properties of VTA/CB− DA neurons showed no

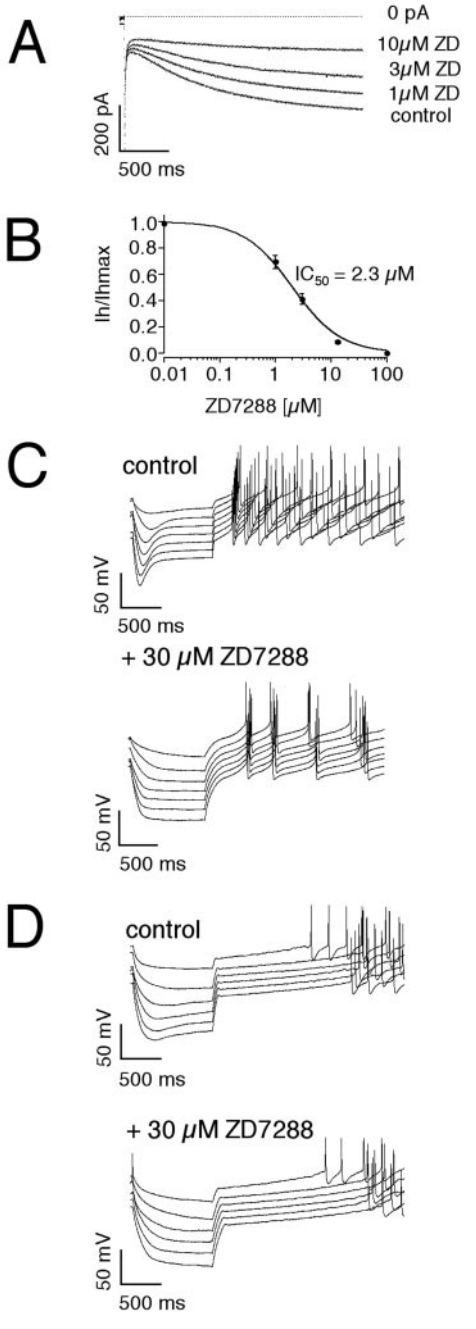

Figure 4. ZD7288-sensitive I_h channels differentially control subthreshold integration in DA subpopulations. *A,* Inhibition of I_h current elicited by a voltage step to −100 mV from a holding potential of −40 mV by 1, 3, and 10 μm ZD7288. *B,* The mean dose–response for ZD7288 inhibition of the I_h current in DA neurons was well described with a single Hill function with an IC_{50} of 2.3 μM and a Hill coefficient of 1.0 ($n = 6$). Current-clamp recordings of membrane responses to injections of increasing hyperpolarizing currents in a SN/CB− neuron (*C*) in comparison with a VTA/CB+ neuron (*D*) under control conditions (*top panel*) and after complete inhibition of I_h channels by 30 μM ZD7288. Although 30 μM ZD7288 completely inhibited the sag component in both SN/CB− and VTA/CB+ neurons, rebound delays and postinhibitory activity is only affected in SN/CB− neurons.

clear trend ($r = 0.08$ for dorsoventral axis and $r = 0.18$ for mediolateral axis) to be associated to their anatomical position within the VTA. CB+ DA neurons in the medial VTA showed the smallest I_h-mediated sag responses during membrane hyper-

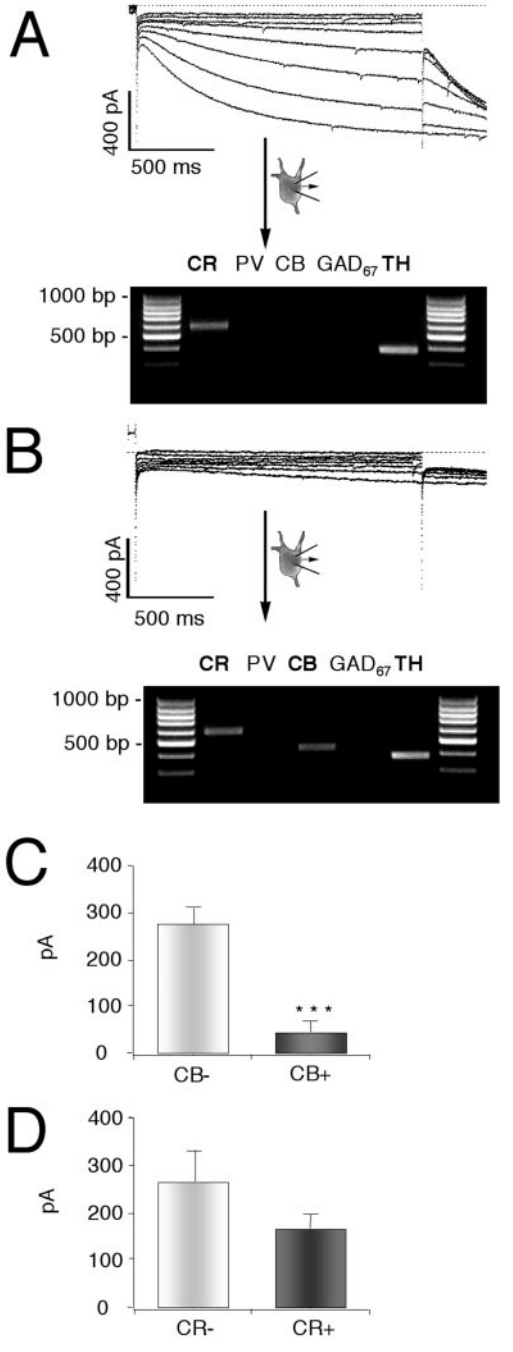

Figure 5. Differential single-cell calbindin mRNA expression in DA neurons is correlated with differences in I_h current amplitudes. *A*, *B,* Single-cell phenotype–genotype correlations in DA neurons comparing I_h currents elicited with 2 sec voltage steps of increasing amplitudes from −50 to −120 mV in steps of 10 mV from a holding potential of −40 mV (*left panels*) with the single-cell mRNA expression profiles of the calcium-binding proteins calretinin (*CR*), parvalbumin (*PV*), and calbindin (*CB*) and the neuronal marker transcripts tyrosine hydroxylase (*TH*) and glutamate decarboxylase (GAD_{67}). The products of the second, nested PCRs were run on a 2% agarose gel in parallel with a 100 bp ladder as molecular weight marker. Two representative examples of DA (TH+) neurons with either large (*A*) or small (*B*) I_h currents and different calcium-binding protein expression profiles, CR (*A*) and CR+CB (*B*), are shown. *C*, *D,* Summaries of phenotype–genotype correlations in DA neurons. Differential single-cell calbindin mRNA expression (*C*) but not that of calretinin (*D*) was correlated with significant differences in I_h current amplitudes in identified DA neurons ($n = 49$). PV was not detected in DA neurons.

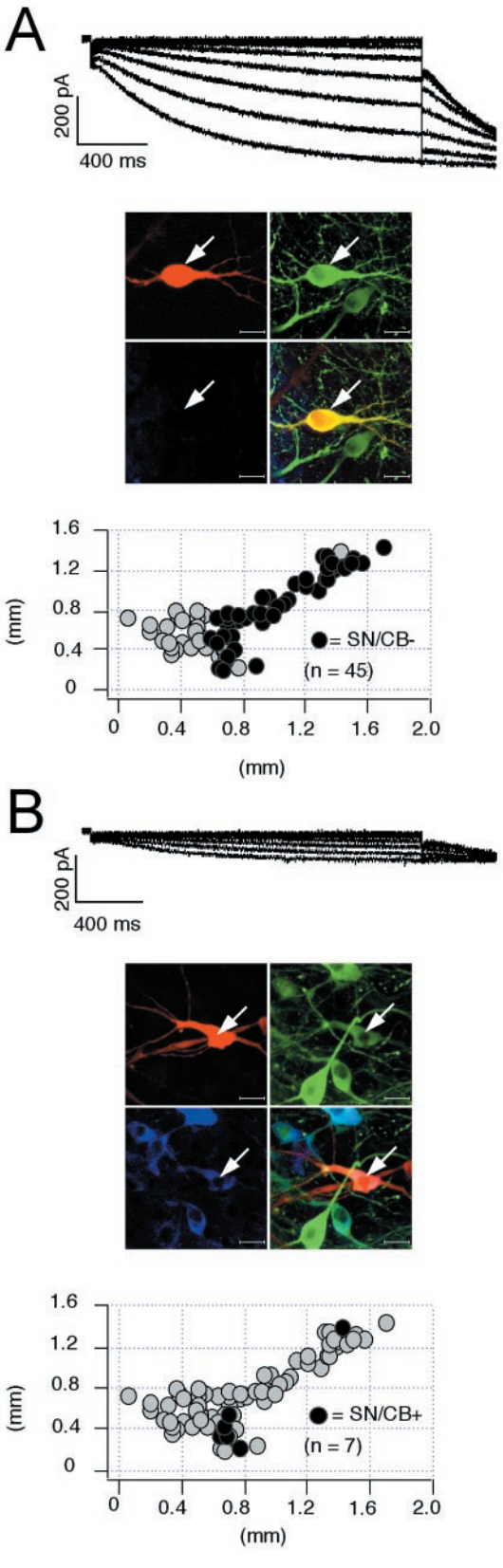

Figure 6. I_h currents in identified SN DA subpopulations. *A*, *B,* Voltage-clamp recordings of I_h currents elicited with 2 sec voltage-steps of increasing amplitudes from −50 to −120 mV in steps of 10 mV from a holding potential of −40 mV (*top panels*) in DA neurons. During recordings neurons were filled with 0.2% neurobiotin. Confocal analysis of coimmunolabeling of recorded neurons (*middle panels*) for neurobiotin (*red, top left*), TH (*green, top right*), and (*blue, bottom left*) identified the recorded cells as a dopaminergic (TH+) and determined anatomical position as well as calbindin expression (*overlay, bottom right, A,* SN/CB−; *B,* SN/CB+). Scale bars, 20 μm. Note larger I_h currents in SN/CB− ($n = 45$) compared with those in SN/CB+ neurons ($n = 7$). Anatomical positions (*black circles*) were plotted in coronal midbrain maps (*bottom panels*) also containing other subpopulations of analyzed DA neurons (*gray circles*).

polarization and their repolarizations were extensively prolonged so that electrical activity was reinitiated only after delays of >1.5 sec (Fig. 2*B,* Table 1). The rebound delays tended to be longer in VTA/CB+ DA neurons that were located closer to the midline of the midbrain ($r = 0.37$). In addition, VTA/CB+ DA neurons had significantly smaller somata compared with the other DA populations (Table 1).

The anatomical distribution of spontaneous pacemaker frequencies recorded from the four identified DA midbrain populations is shown in Figure 3*A*. VTA/CB+ DA neurons possessed significantly faster pacemaker frequencies of ~5.2 Hz compared with the other three identified DA populations that discharged with mean frequencies between 2.4 and 3.6 Hz (Table 1). As shown in Figure 3*B*, there was a strong linear correlation ($r = 0.98$) between the mean discharge frequencies of the four DA subpopulations and their mean peak amplitude of AHPs. Figure 3*C* displays the anatomical distribution of postinhibitory rebound delays in midbrain DA neurons with fast firing VTA/CB+ DA neurons showing the longest rebound delays. Figure 3*D* plots the strong inverse linear correlation ($r = 0.95$) between the mean amplitudes of the sag repolarization and the mean duration of the rebound delay before reinitiating pacemaker activity. As illustrated in Figure 3*E*, differences in sag depolarizations during membrane hyperpolarization also affected the discharge once the firing threshold was crossed. Although SN/CB− DA neurons demonstrated a transient phase of postinhibition excitation, faster discharging VTA/CB+ DA neurons displayed a pronounced postinhibition rebound delay. Once their pacemaker set in, firing frequency was stable.

Current-clamp recordings of different DA subpopulations demonstrated significant differences in the amplitudes of sag repolarizations. This suggested that I_h channels contribute to their functional differences. To define the functional contribution of I_h channels, we characterized the pharmacological profile of native I_h currents in voltage-clamp recordings. I_h currents in DA neurons in the SN and VTA were reversibly blocked by similar concentrations of cesium (SN: $IC_{50} = 89.4 \pm 8.7$ μM, $n = 6$; VTA: $IC_{50} = 93.3 \pm 11.9$ μM, $n = 6$, data not shown). In agreement with a previous study (Mercuri et al., 1995), higher concentration of cesium ions (>0.5 mm) also blocked time-independent currents in DA neurons (data not shown). The I_h channel inhibitor ZD7288 also blocked Ih currents in DA neurons with an IC_{50} of 2.3 ± 0.4 μM (Fig. 4*A,B*) ($n = 6$). Current-clamp recordings demonstrated that 30 μM ZD7288 completely inhibited sag depolarizations in different types of DA neurons (Fig. 4*C,D*). Higher ZD7288 concentrations (>100 μM) additionally perturbed the pacemaker mechanism and electrically silenced DA neurons (data not shown). These experiments confirmed that the sag depolarization in DA subpopulations were solely mediated by ZD7288-sensitive I_h channels. In SN/CB− neurons, ZD7288 not only inhibited the large sag component, but the rebound delay was also significantly prolonged, and the transient posthyperpolarization excitation was lost. With complete I_h channel inhibition, the

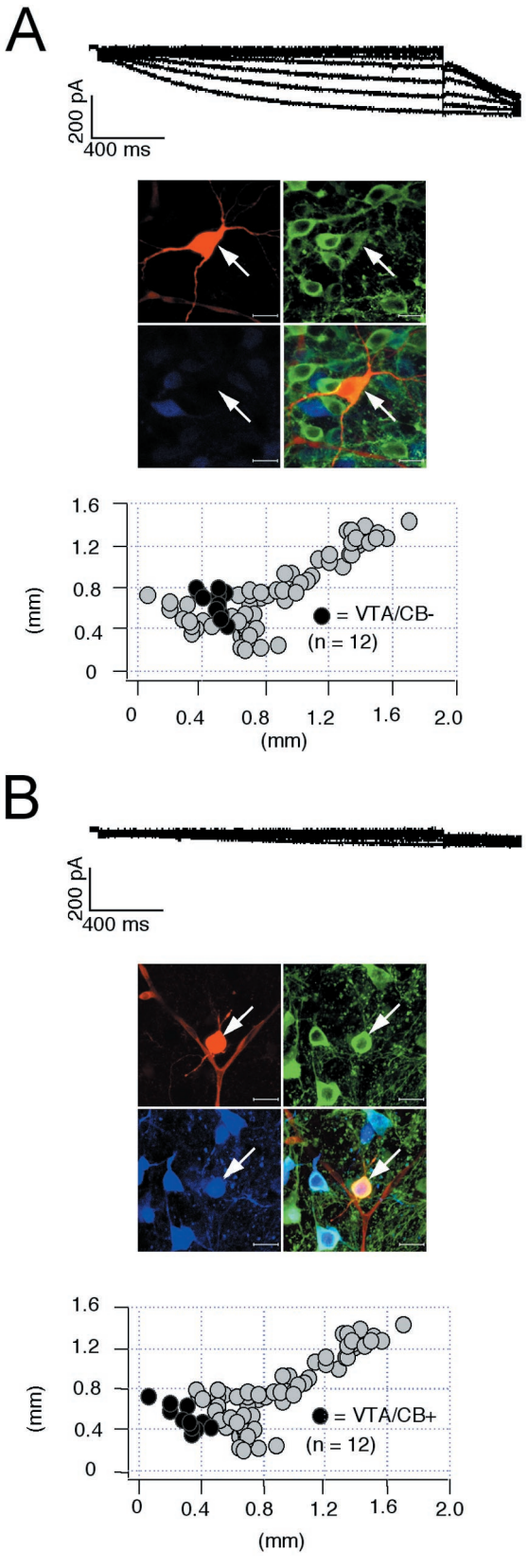

Figure 7. I_h currents in identified VTA DA subpopulations. *A*, *B,* Voltage-clamp recordings of I_h currents elicited with 2 sec voltage steps of increasing amplitudes from −50 to −120 mV in steps of 10 mV from a holding potential of −40 mV (*top panels*) in DA neurons. During recordings neurons were filled with 0.2% neurobiotin. Confocal analysis of coimmunolabeling of recorded neurons (*middle panels*) for neurobiotin (*red, top left*), TH (*green, top right*), and CB (*blue, bottom left*) identified the recorded cells as a dopaminergic (TH+) and determined anatomical position as well as calbindin expression (*overlay, bottom right, A,* VTA/CB−; *B,* VTA/CB+). Scale bars, 20 μm. Note larger I_h currents in VTA/CB− (n = 12) compared with those in VTA/CB+ neurons (n = 12). Anatomical positions (*black circles*) were plotted in coronal midbrain maps (*bottom panels*) also containing other subpopulations of analyzed DA neurons (*gray circles*).

timing of action potentials became independent of the preceding membrane potential (Fig. 4*C*) (n = 10). In contrast, although in VTA/CB+ DA neurons 30 μM ZD7288 completely inhibited the smaller sag component, I_h channel inhibition did not affect rebound delays and postinhibitory timing of action potentials (Fig. 4*D*) (n = 12). In these neurons membrane hyperpolarization beyond a sharp threshold was linked to a long and rigid pause before reinitiation of firing.

To determine whether there was a specific correlation between I_h current amplitudes and the differential expression of relevant calcium-binding proteins, we performed single-cell RT-PCR experiments (Lambolez et al., 1992; Cauli et al., 1997; Liss et al., 1999a) to compare the mRNA expression profiles of these calcium-binding proteins with amplitudes of I_h currents in individual DA neurons (n = 49). We probed for CB, CR, and PV, as well as for the dopaminergic marker TH and the GABAergic marker L-glutamate decarboxylase (GAD_{67}). While PV was expressed in GABAergic midbrain neurons (data not shown), we detected differential expression of calbindin and calretinin mRNA in TH+ SN and VTA neurons. Thirty-five percent of the analyzed DA neurons were CB+ (n = 17 of 49), and most (88%) of these also coexpressed CR (n = 15 of 17). However, only 47% of the CB− neurons were also CR− (n = 15 of 32), demonstrating that coexpression of CB and CR was not correlated on the level of single DA neurons. Moreover, the differential expression of CB but not that of CR was correlated with significant differences in I_h current amplitudes (Fig. 5). Consistent with our immunocytochemical data, large I_h currents were detected in calbindin mRNA-negative DA neurons, although calbindin mRNA-positive DA neurons possessed significantly smaller I_h currents. These single-cell mRNA expression data confirm that calbindin but not calretinin is a specific marker for functionally distinct subpopulations of DA midbrain neurons.

The amplitude of the sag component recorded in current-clamp was not necessarily a direct indicator of the size of I_h currents but might, for instance, also be affected by other conductances in the subthreshold range. Thus, we activated I_h currents in the voltage-clamp configuration by 2 sec hyperpolarizing voltage steps of increasing amplitude (−50 to −120 mV) from a holding potential of −40 mV and filled these recorded neurons for anatomical and neurochemical identification as described above. Significant differences in I_h current amplitudes were indeed present in the four DA subpopulations (Figs. 6, 7). Consistent with our current-clamp data (Figs. 1, 2), SN/CB− neurons displayed the largest I_h currents (Fig. 6*A*) (n = 45), followed by VTA/CB− cells (Fig. 7*A*) (n = 12). The CB+ DA subpopulations in SN and VTA possessed significantly smaller I_h currents (Fig. 6*B*) (n = 7) (Fig. 7*B*) (n = 12). In contrast to the differences in current amplitudes between the DA subpopulations, we detected no significant differences in the voltage dependence (SN/CB−: V_{50} = −98.1 ± 1 mV, slope = 8.9 ± 0.3 mV, n = 42; SN/CB+: V_{50} = −99.2 ± 1.9 mV, slope = 7.4 ± 0.9 mV, n = 5; VTA/CB−: V_{50} = −99.6 ± 2

mV, slope = 8.6 ± 0.8 mV, n = 9; VTA/CB+: V_{50} = −100.3 ± 1.3 mV, slope = 8.7 ± 0.8 mV, n = 11). Also, no significant differences in the gating kinetics of I_h currents between SN/CB−, SN/CB+, and VTA/CB− neurons were found. In VTA/CB+ neurons however, I_h activated with ~1.6-fold slower time constants [SN/CB−: tau-1 (at −120 mV), 796.8 ± 36.1 msec, n = 45; SN/CB+: tau-1 (at −120 mV), 753.4 ± 115.4 msec, n = 7; VTA/CB−: tau-1 (at −120 mV), 843.9 ± 85.8 msec, n = 11; VTA/CB+: tau-1 (at −120 mV), 1286.3 ± 116.3 msec, n = 12]. To account for the small differences in I_h activation kinetics and cell sizes between the different DA populations, we integrated the I_h currents activated at −120 mV to calculate I_h charge transfer (in picocoulombs; see Materials and Methods) and normalized them to cell size (picofarads). Figure 8*A* shows the anatomical distribution of these I_h charge transfer densities (picocoulombs per picofarad) for DA midbrain neurons. The strong inverse linear correlation (r = 0.95) between the mean I_h charge transfer densities (picocoulombs per picofarad) and the rebound delays (in milliseconds) of the four subpopulations of DA neurons demonstrated that I_h channels are involved in the observed differences of postinhibition behavior of DA neurons (Fig. 8*B*). In contrast, we found no differences in the time-independent leak densities (picocoulombs per picofarad) between DA subpopulations (Fig. 8*C,D*), which were calculated from the time-independent currents evoked by membrane hyperpolarizations to −120 mV.

Finally, the question remained whether the observed differences in I_h charge densities were also involved in the control of the pacemaker. The voltage dependence and gating of I_h channels is temperature-sensitive and modulated by several factors, including cyclic nucleotides (Pape, 1996). Thus, we used the gramicidin-perforated patch technique for this set of experiments and recorded the effect of I_h channel inhibition by 30 μM ZD7288 on spontaneous pacemaker activity at 35°C. To identify the anatomical position and calbindin expression of the DA neurons, we converted the perforated patch to the standard-whole cell configuration at the end of the experiments, labeled the recorded neuron, and processed it as described above. As evident from Figures 9 and 10, only in SN/CB− DA neurons did I_h channels actively control the frequency of the intrinsic pacemaker. Their inhibition led to a significant reduction in discharge rate (SN/CB−: −43.1 ± 6.3%, n = 7). I_h channel inhibition significantly altered the frequency of spontaneous electrical activity in none of the other three DA subpopulations that either also fired in a regular pacemaker mode (SN/CB+;VTA/CB−: 2.4 ± 0.3 Hz; 3.6 ± 0.3 Hz, n = 11) or that showed a more irregular discharge mode (VTA/CB+, 5.2 ± 0.6 Hz, n = 6) (Wolfart et al., 2001).

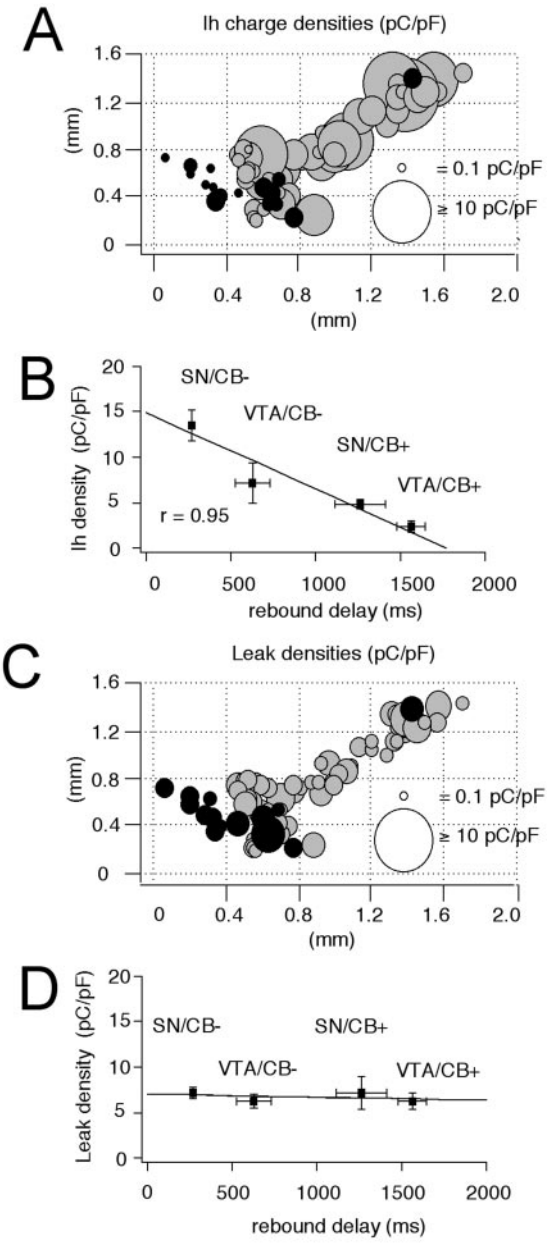

Figure 8. Differences in I_h charge densities contribute to distinct rebound delays in DA subpopulations. *A,* Anatomical distribution of I_h charge densities (in picocoulombs per picofarad; see Materials and Methods) in immunohistochemically characterized and identified DA neurons (n = 75). CB+ neurons are represented by *black circles*, and CB− neurons are represented by *gray circles*. I_h density is coded by symbol size (0.1–20 pC/pF) and are significantly different between all four DA subpopulations. *B,* Linear scaling between mean I_h charge densities and respective mean rebound delays (r = 0.95) in DA subpopulations. *C,* Anatomical distribution of time-independent leak charge densities (in picocoulombs per picofarad; see Materials and Methods) in immunohistochemically characterized and identified DA neurons (n = 75). CB+ neurons are represented by *black circles*, and CB− neurons are represented by *gray circles*. Leak density is coded by symbol size. *D,* No differences in leak densities were detected in DA subpopulations and differences in rebound behavior are independent of time-independent leak charge density.

DISCUSSION

Functional diversity of anatomically and neurochemically identified DA midbrain neurons

The localization of recorded DA neurons in the SN or VTA in combination with their differential CB expression were used to discriminate four DA midbrain populations: SN/CB−, SN/CB+, VTA/CB−, and VTA/CB+. The relative abundance of detected CB+ and CB− DA neurons in both SN and VTA is consistent with previous immunohistochemical (Liang et al., 1996) and single-cell RT-PCR studies (Klink et al., 2001). We show here that these neurochemically and anatomically identified DA subpopulations possess significant electrophysiological differences in particular in response to hyperpolarizing current injections and in pacemaker frequency control. In contrast within individual neurochemically defined DA subpopulations, variations of these functional properties were not strongly correlated to their mediolateral or ventrodorsal positions within the respective nucleus. The anatomical distributions of these functionally and neurochemically distinct DA subpopulations are correlated to the an-

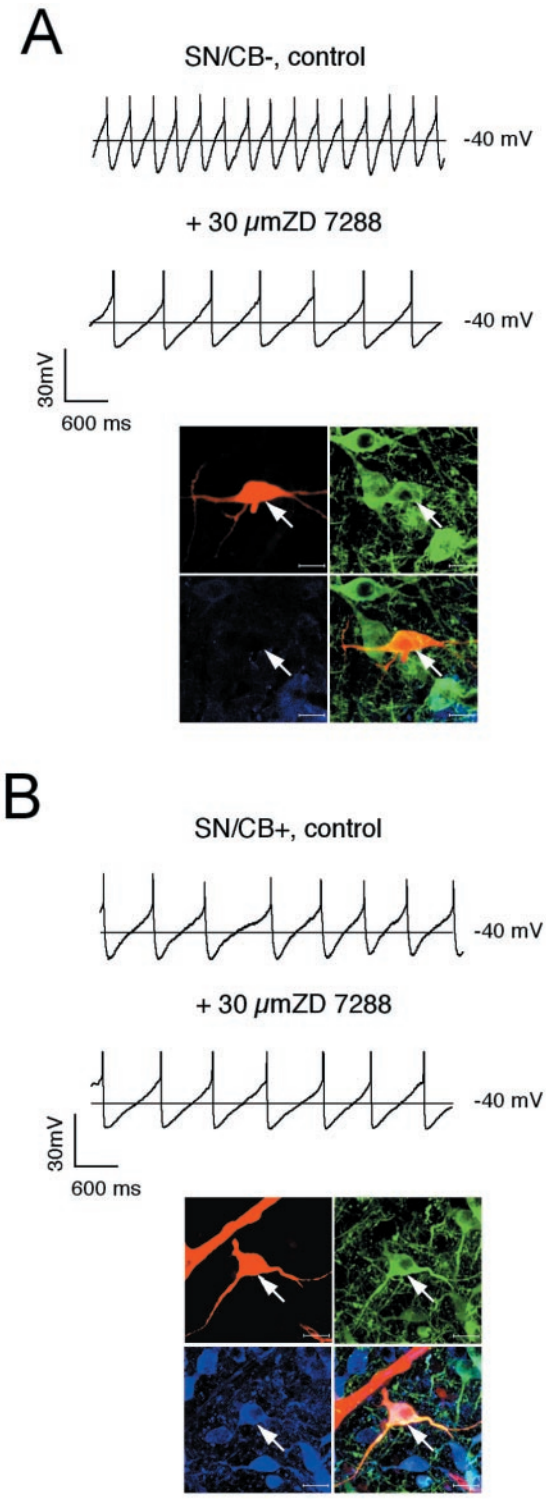

Figure 9. Subpopulation-selective pacemaker control by I_h channels in SN. *A*, *B,* Current-clamp recordings in the gramicidin-perforated patch configuration at physiological temperatures in control and after application of 30 μM ZD7288 (*top panels*) in DA neurons. At the end of the experiment, the perforated-patch was converted to the standard whole-cell configuration, and the neurons were filled with 0.2% neurobiotin. Confocal analysis of coimmunolabeling of recorded neurons (*bottom panels*) for neurobiotin (*red, top left*), TH (*green, top right*), and CB (*blue, bottom left*) identified the recorded cells as a dopaminergic (TH+) and determined calbindin expression (*overlay, bottom right, A,* SN/CB−; *B,* SN/CB+). Scale bars, 20 μm. I_h channels control pacemaker frequencies only in SN/CB− (*A*) but not in SN/CB+ (*B*).

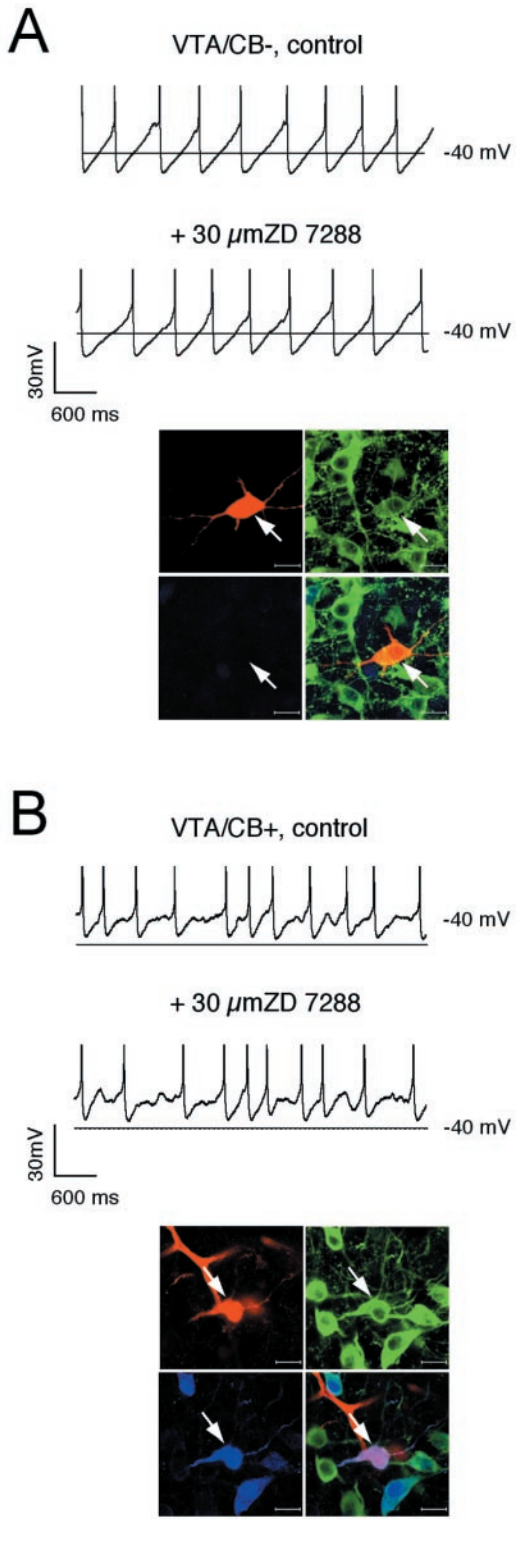

Figure 10. I_h channels do not control pacemaker frequency in VTA DA neurons. *A*, *B,* Current-clamp recordings in the gramicidin-perforated patch configuration at physiological temperatures in control and after application of 30 μM ZD7288 (*top panels*) in DA neurons. At the end of the experiment, the perforated-patch was converted to the standard whole-cell configuration, and the neurons were filled with 0.2% neurobiotin. Confocal analysis of coimmunolabeling of recorded neurons (*bottom panels*) for neurobiotin (*red, top left*), TH (*green, top right*), and CB (*blue, bottom left*) identified the recorded cells as a dopaminergic (TH+) and determined calbindin expression (*overlay, bottom right, A,* VTA/CB−; *B,* VTA/CB+). Scale bars, 20 μm.

atomical topography of DA midbrain systems (Gerfen, 1992b; Maurin et al., 1999; Haber et al., 2000; Joel and Weiner, 2000). This might suggest that DA populations with distinct axonal targets, like CB+ and CB− SN neurons, possess also different postsynaptic properties. In the VTA, the distribution of CB+ DA neurons that displayed the most distinct phenotype with irregular discharge at higher frequencies combined with a prolonged postinhibitory hypoexcitability best matched the localization of mesoprefrontal DA neurons (Chiodo et al., 1984; Gariano et al., 1989). In contrast, the larger, calbindin-negative (VTA/CB−) DA neurons are more likely to constitute the mesolimbic projections (Swanson, 1982; Oades and Halliday, 1987; Carr and Sesack, 2000a). However, verification must come from the direct functional analysis of retrogradely labeled DA midbrain neurons.

Differences in I_h currents contribute to selective pacemaker control and subthreshold properties in identified DA subpopulations

Our study provides evidence that DA midbrain subpopulations significantly diverge from a single electrophysiological phenotype (Kitai et al., 1999). We identified differences in I_h current expressed as significant differences in I_h charge densities as an important mechanism responsible for functional diversity of DA neurons. Under the assumption of similar unitary I_h channel properties, these different I_h charge densities would correspond to different densities of functional I_h channels. The underlying molecular differences remain to be defined. Qualitative single-cell RT-mPCR experiments have shown that DA SN neurons coexpress three of the four I_h channel subunits, HCN2, HCN3, and HCN4 (Franz et al., 2000). However, the molecular composition of native neuronal I_h channels that might exist as homomeric or heteromeric complexes (Chen et al., 2001; Ulens and Tytgat, 2001; Yu et al., 2001) as well as the possible differential I_h channel subunit expression between different DA subpopulations remains unclear. In this context, quantitative differences in HCN subunit expression might also play a significant role. Relevant functional differences in subthreshold behavior remain even during complete inhibition of I_h channels between the different DA subpopulations. This indicates that other ion channels are also differentially expressed in distinct DA populations, as we have previously described for SK3 channels (Wolfart et al., 2001). The irregular firing DA VTA neurons with low SK3 channel density (Wolfart et al., 2001) are likely to correspond to the calbindin-positive VTA subpopulation delineated in this study. In addition, we have recently shown by quantitative single-cell real-time PCR that differences in transcript numbers for Kv4α and Kv4β subunits control the A-type potassium channel density and pacemaker frequency in DA SN neurons (Liss et al., 2001). Other obvious candidates that might contribute to functional diversity are persistent sodium channels (Grace, 1991; Catterall, 2000; Maurice et al., 2001) and low-threshold calcium channels (Kang and Kitai, 1993; Cardozo and Bean, 1995; Perez-Reyes, 1999).

What are the functional implications of these I_h channel-mediated differences in DA neurons? We show that only in SN/CB− neurons I_h channels are directly involved in pacemaker frequency control. Similar results have been obtained by extracellular recordings in DA neurons (Seutin et al., 2001). Selective pacemaker control by I_h channels has two important consequences. First, because I_h channels significantly contribute to the resonance profile of neurons (Hutcheon and Yarom, 2000), the active I_h channel pool will selectively increase the stability of regular, tonic discharge in SN/CB− DA neurons. I_h channels are likely to do this in concert with the high density of calcium-activated SK3 channels that are also present in these SN neurons and also control frequency and stability of the pacemaker (Wolfart et al., 2001). *In vivo* studies have shown that this DA subtype discharges more regularly and less often in burst mode compared with VTA DA neurons (Chiodo et al., 1984; Grace and Bunney, 1984a,b; Greenhoff et al., 1988). In this context, it is important that the transition between single spike and burst mode (i.e., tonic and phasic DA signaling) are regarded as an essential element in the signal processing of the DA system (Schultz, 1998; Waelti et al., 2001). Second, I_h channels are directly modulated by cyclic nucleotides (Wainger et al., 2001) and thus are potential targets of many signaling cascades that control cyclic nucleotide levels in neurons (Pape, 1996; Luthi and McCormick, 1999; Budde et al., 2000). Thus, SN/CB− neurons are likely to be particularly sensitive to neuromodulatory input by for instance, serotonin (Nedergaard et al., 1991; Kitai et al., 1999).

In addition to pacemaker control, the differences in I_h channel density will also lead to distinct modes of phasic postsynaptic integration. Whereas SN/CB− DA neurons show an I_h channel-dependent transient, postinhibitory excitation, VTA/CB+ DA neurons display a pronounced postinhibitory inhibition. These results indicate that the differences in I_h channel density in DA neurons might be important for the integration of GABAergic signaling, which represents the most abundant (>70%) synaptic input to DA neurons (Grace and Bunney, 1985; Bolam et al., 2000). These postsynaptic differences are well suited to amplify the different pattern of GABA-mediated indirect rebound excitation or direct inhibition that have both been observed in DA neurons *in vivo* (Kiyatkin and Rebec, 1998; Paladini et al., 1999). In addition, differences in I_h channel density are also likely to affect the temporal structure of synaptic integration (Magee, 1999). It has been postulated that SN/CB− DA neurons operate in a closed striato-nigro-striatal loop providing phasic DA release induced by concerted and precisely timed disinhibition from nigral and pallidal GABAergic input, whereas SN/CB+ DA neurons as well as VTA DA neurons are directly inhibited by striatal input in a open-loop configuration with less temporal precision (Maurin et al., 1999; Joel and Weiner, 2000). Our data suggest that the differences in I_h channel density could contribute to the different polarity and temporal structure of GABAergic integration in DA neurons.

Differential vulnerabilities to neurodegeneration of DA midbrain neurons are associated with distinct functional phenotypes

Anatomical position and differential expression of calbindin were shown to be associated with differential vulnerability of DA neurons to neurodegeneration in Parkinson's disease and its related animal models (Gaspar et al., 1994; German et al., 1996; Liang et al., 1996; Damier et al., 1999; Prensa et al., 2000; Tan et al., 2000). There is consensus that the calbindin-negative SN neurons are significantly more vulnerable compared with the calbindin-positive SN/CB+ and VTA neurons. However, studies on the calbindin-KO mouse have shown that this protein is not causally involved in conferring resistance to neurotoxins and thus might only be used as a marker for less vulnerable cells in the SN (Airaksinen et al., 1997). In this context, it is noteworthy that only the highly vulnerable class of DA neurons possesses the strong rebound activation, which might render these neurons more susceptible to glutamatergic input (Beal, 2000). In addition, the most vulnerable DA neurons possess the highest density of I_h channels.

Mitochondrial dysfunction, which is regarded as an important trigger factor of Parkinson's disease (Greenamyre et al., 1999; Beal, 2000; Betarbet et al., 2000), might lead to tonic activation of ATP-sensitive potassium (K-ATP) channels and consequently to chronic membrane hyperpolarization (Liss et al., 1999b). Indeed, this tonic activation of K-ATP channels has been demonstrated in DA neurons in the *weaver* mouse, a genetic model of dopaminergic neurodegeneration (Liss et al., 1999a). However, K-ATP channel-mediated membrane hyperpolarization will activate I_h channels and thus counteract hyperpolarization and also lead to sodium loading (Tsubokawa et al., 1999; Guatteo et al., 1998, 2000). Thus, differential density of I_h channels in DA neurons might result in different pathophysiological responses to metabolic stress and in this way contribute to the differential vulnerability of DA neurons to neurodegeneration.

REFERENCES

Airaksinen MS, Thoenen H, Meyer M (1997) Vulnerability of midbrain dopaminergic neurons in calbindin-D28k-deficient mice: lack of evidence for a neuroprotective role of endogenous calbindin in MPTP-treated and weaver mice. Eur J Neurosci 9:120–127.

Akaike N (1999) Gramicidin perforated patch recording technique. Nippon Yakurigaku Zasshi 113:339–347.

Barrot M, Calza L, Pozza M, Le Moal M, Piazza PV (2000) Differential calbindin-immunoreactivity in dopamine neurons projecting to the rat striatal complex. Eur J Neurosci 12:4578–4582.

Beal MF (2000) Energetics in the pathogenesis of neurodegenerative diseases. Trends Neurosci 23:298–304.

Berke JD, Hyman SE (2000) Addiction, dopamine, the molecular mechanisms of memory. Neuron 25:515–532.

Betarbet R, Sherer TB, MacKenzie G, Garcia-Osuna M, Panov AV, Greenamyre JT (2000) Chronic systemic pesticide exposure reproduces features of Parkinson's disease. Nat Neurosci 3:1301–1306.

Bolam JP, Hanley JJ, Booth PA, Bevan MD (2000) Synaptic organisation of the basal ganglia. J Anat 196:527–542.

Budde T, Sieg F, Braunewell KH, Gundelfinger ED, Pape HC (2000) Ca^{2+}-induced Ca^{2+} release supports the relay mode of activity in thalamocortical cells. Neuron 26:483–492.

Cardozo DL, Bean BP (1995) Voltage-dependent calcium channels in rat midbrain dopamine neurons: modulation by dopamine and GABAB receptors. J Neurophysiol 74:1137–1148.

Carr DB, Sesack SR (2000a) GABA-containing neurons in the rat ventral tegmental area project to the prefrontal cortex. Synapse 38:114–123.

Carr DB, Sesack SR (2000b) Projections from the rat prefrontal cortex to the ventral tegmental area: target specificity in the synaptic associations with mesoaccumbens and mesocortical neurons. J Neurosci 20:3864–3873.

Catterall WA (2000) From ionic currents to molecular mechanisms: the structure and function of voltage-gated sodium channels. Neuron 26:13–25.

Cauli B, Audinat E, Lambolez B, Angulo MC, Ropert N, Tsuzuki K, Hestrin S, Rossier J (1997) Molecular and physiological diversity of cortical nonpyramidal cells. J Neurosci 17:3894–3906.

Chen S, Wang J, Siegelbaum SA (2001) Properties of hyperpolarization-activated pacemaker current defined by coassembly of HCN1 and HCN2 subunits and basal modulation by cyclic nucleotide. J Gen Physiol 117:491–504.

Chiodo LA, Bannon MJ, Grace AA, Roth RH, Bunney BS (1984) Evidence for the absence of impulse-regulating somatodendritic and synthesis-modulating nerve terminal autoreceptors on subpopulations of mesocortical dopamine neurons. Neuroscience 12:1–16.

Damier P, Hirsch EC, Agid Y, Graybiel AM (1999) The substantia nigra of the human brain. I. Nigrosomes and the nigral matrix, a compartmental organization based on calbindin D(28K) immunohistochemistry. Brain 122:1421–1436.

Dunnet SB, Bjorklund A (1999) Prospects for new restorative and neuroprotective treatments in Parkinson's disease. Nature 399:A32–A39.

Fallon JH (1988) Topographic organization of ascending dopaminergic projections. Ann NY Acad Sci 537:1–9.

Francois C, Yelnik J, Tande D, Agid Y, Hirsch EC (1999) Dopaminergic cell group A8 in the monkey: anatomical organization and projections to the striatum. J Comp Neurol 414:334–347.

Franz O, Liss B, Neu A, Roeper J (2000) Single-cell mRNA expression of HCN1 correlates with a fast gating phenotype of hyperpolarization-activated cyclic nucleotide-gated ion channels (I_h) in central neurons. Eur J Neurosci 12:2685–2693.

Gariano RF, Tepper JM, Sawyer SF, Young SJ, Groves PM (1989) Mesocortical dopaminergic neurons. 1. Electrophysiological properties and evidence for soma-dendritic autoreceptors. Brain Res Bull 22:511–516.

Gaspar P, Ben Jelloun N, Febvret A (1994) Sparing of the dopaminergic neurons containing calbindin-D28k and of the dopaminergic mesocortical projections in weaver mutant mice. Neuroscience 61:293–305.

Gerfen CR (1992a) The neostriatal mosaic: multiple levels of compartmental organization. J Neural Transm Suppl 36:43–59.

Gerfen CR (1992b) The neostriatal mosaic: multiple levels of compartmental organization in the basal ganglia. Annu Rev Neurosci 15:285–320.

German DC, Nelson EL, Liang CL, Speciale SG, Sinton CM, Sonsalla PK (1996) The neurotoxin MPTP causes degeneration of specific nucleus A8, A9 and A10 dopaminergic neurons in the mouse. Neurodegeneration 5:299–312.

Goldman-Rakic PS (1999) The physiological approach: functional architecture of working memory and disordered cognition in schizophrenia. Biol Psychiatry 46:650–661.

Gonzalez-Hernandez T, Rodriguez M (2000) Compartmental organization and chemical profile of dopaminergic and GABAergic neurons in the substantia nigra of the rat. J Comp Neurol 421:107–135.

Grace AA (1991) Regulation of spontaneous activity and oscillatory spike firing in rat midbrain dopamine neurons recorded in vitro. Synapse 7:221–234.

Grace AA (2000) The tonic/phasic model of dopamine system regulation and its implications for understanding alcohol and psychostimulant craving. Addiction 95 Suppl 2:S119–128.

Grace AA, Bunney BS (1984a) The control of firing pattern in nigral dopamine neurons: burst firing. J Neurosci 4:2877–2890.

Grace AA, Bunney BS (1984b) The control of firing pattern in nigral dopamine neurons: single spike firing. J Neurosci 4:2866–2876.

Grace AA, Bunney BS (1985) Opposing effects of striatonigral feedback pathways on midbrain dopamine cell activity. Brain Res 333:271–284.

Grace AA, Onn SP (1989) Morphology and electrophysiological properties of immunocytochemically identified rat dopamine neurons recorded in vitro. J Neurosci 9:3463–3481.

Greenamyre JT, MacKenzie G, Peng TI, Stephans SE (1999) Mitochondrial dysfunction in Parkinson's disease. Biochem Soc Symp 66:85–97.

Greenhoff J, Ugedo L, Svensson TH (1988) Firing pattern of midbrain dopamine neurons: differences between A9 and A10 cells. Acta Physiol Scand 134:127–132.

Guatteo E, Mercuri NB, Bernardi G, Knopfel T (1998) Intracellular sodium and calcium homeostasis during hypoxia in dopamine neurons of rat substantia nigra pars compacta. J Neurophysiol 80:2237–2243.

Guatteo E, Fusco FR, Giacomini P, Bernardi G, Mercuri NB (2000) The weaver mutation reverses the function of dopamine and GABA in mouse dopaminergic neurons. J Neurosci 20:6013–6020.

Haber SN, Fudge JL, McFarland NR (2000) Striatonigrostriatal pathways in primates form an ascending spiral from the shell to the dorsolateral striatum. J Neurosci 20:2369–2382.

Hanley JJ, Bolam JP (1997) Synaptology of the nigrostriatal projection in relation to the compartmental organization of the neostriatum in the rat. Neuroscience 81:353–370.

Hutcheon B, Yarom Y (2000) Resonance, oscillation, the intrinsic frequency preferences of neurons Trends Neurosci 23:216–222.

Joel D, Weiner I (2000) The connections of the dopaminergic system with the striatum in rats and primates: an analysis with respect to the functional and compartmental organization of the striatum. Neuroscience 96:451–474.

Kang Y, Kitai ST (1993) A whole cell patch-clamp study on the pacemaker potential in dopaminergic neurons of rat substantia nigra compacta. Neurosci Res 18:209–221.

Kitai ST, Shepard PD, Callaway JC, Scroggs R (1999) Afferent modulation of dopamine neuron firing patterns. Curr Opin Neurobiol 9:690–697.

Kiyatkin EA, Rebec GV (1998) Heterogeneity of ventral tegmental area neurons: single-unit recording and iontophoresis in awake, unrestrained rats. Neuroscience 85:1285–1309.

Klink J, de Kerchove d'Exaerde A, Zoli M, Changeux J-P (2001) Molecular and physiological diversity of nicotinic acetylcholine receptors in the midbrain dopaminergic nuclei. J Neurosci 21:1452–1463.

Lacey MG, Mercuri NB, North RA (1989) Two cell types in rat substantia nigra zona compacta distinguished by membrane properties and the actions of dopamine and opioids. J Neurosci 9:1233–1241.

Lambolez B, Audinat E, Bochet P, Crepel F, Rossier J (1992) AMPA receptor subunits expressed by single Purkinje cells. Neuron 9:247–258.

Liang CL, Sinton CM, German DC (1996) Midbrain dopaminergic neurons in the mouse: co-localization with calbindin-D28K and calretinin. Neuroscience 75:523–533.

Liss B, Neu A, Roeper J (1999a) The weaver mouse gain-of-function phenotype of dopaminergic midbrain neurons is determined by coactivation of wvGirk2 and K-ATP channels. J Neurosci 19:8839–8848.

Liss B, Bruns R, Roeper J (1999b) Alternative sulfonylurea receptor expression defines metabolic sensitivity of K-ATP channels in dopaminergic midbrain neurons. EMBO J 18:833–846.

Liss B, Franz O, Sewing S, Bruns R, Neuhoff H, Roeper J (2001) Tuning the pacemaker frequency of individual dopaminergic neurons by variable Kv4.3L and KChip3.1 transcript numbers. EMBO J 20:5715–5724.

Luthi A, McCormick DA (1999) Modulation of a pacemaker current through Ca(2+)-induced stimulation of cAMP production. Nat Neurosci 2:634–641.

Magee JC (1999) Dendritic I_h normalizes temporal summation in hippocampal CA1 neurons. Nat Neurosci 2:848.

Maurice N, Tkatch T, Meisler M, Sprunger LK, Surmeier DJ (2001) D1/D5 dopamine receptor activation differentially modulates rapidly inactivating and persistent sodium currents in prefrontal cortex pyramidal neurons. J Neurosci 21:2268–2277.

Maurin Y, Banrezes B, Menetrey A, Mailly P, Deniau JM (1999) Three-dimensional distribution of nigrostriatal neurons in the rat: relation to the topography of striatonigral projections. Neuroscience 91:891–909.

Mercuri NB, Bonci A, Calabresi P, Stefani A, Bernardi G (1995) Properties of the hyperpolarization-activated cation current I_h in rat midbrain dopaminergic neurons. Eur J Neurosci 7:462–469.

Nedergaard S, Flatman JA, Engberg I (1991) Excitation of substantia nigra pars compacta neurones by 5-hydroxy-tryptamine in vitro. NeuroReport 2:329–332.

Oades RD, Halliday GM (1987) Ventral tegmental (A10) system: neurobiology. 1. Anatomy and connectivity. Brain Res 434:117–165.

Paladini CA, Tepper JM (1999) GABA(A) and GABA(B) antagonists differentially affect the firing pattern of substantia nigra dopaminergic neurons in vivo. Synapse 32:165–176.

Paladini CA, Celada P, Tepper JM (1999) Striatal, pallidal, and pars reticulata evoked inhibition of nigrostriatal dopaminergic neurons is mediated by GABA(A) receptors in vivo. Neuroscience 89:799–812.

Pape HC (1996) Queer current and pacemaker: the hyperpolarization-activated cation current in neurons. Annu Rev Physiol 58:299–327.

Perez-Reyes E (1999) Three for T: molecular analysis of the low voltage-activated calcium channel family. Cell Mol Life Sci 56:660–669.

Prensa L, Cossette M, Parent A (2000) Dopaminergic innervation of human basal ganglia. J Chem Neuroanat 20:207–213.

Pucak ML, Grace AA (1994) Regulation of substantia nigra dopamine neurons. Crit Rev Neurobiol 9:67–89.

Richards CD, Shiroyama T, Kitai ST (1997) Electrophysiological and immunocytochemical characterization of GABA and dopamine neurons in the substantia nigra of the rat. Neuroscience 80:545–557.

Sanghera MK, Trulson ME, German DC (1984) Electrophysiological properties of mouse dopamine neurons: in vivo and in vitro studies. Neuroscience 12:793–801.

Santoro B, Tibbs GR (1999) The HCN gene family: molecular basis of the hyperpolarization-activated pacemaker channels. Ann N Y Acad Sci 868:741–764.

Schultz W (1998) Predictive reward signal of dopamine neurons. J Neurophysiol 80:1–27.

Seutin V, Massotte L, Renette MF, Dresse A (2001) Evidence for a modulatory role of I_h on the firing of a subgroup of midbrain dopamine neurons. NeuroReport 12:255–258.

Shepard PD, German DC (1988) Electrophysiological and pharmacological evidence for the existence of distinct subpopulations of nigrostriatal dopaminergic neuron in the rat. Neuroscience 27:537–546.

Spanagel R, Weiss F (1999) The dopamine hypothesis of reward: past and current status. Trends Neurosci 22:521–527.

Stuart GJ, Dodt HU, Sakmann B (1993) Patch-clamp recordings from the soma and dendrites of neurons in brain slices using infrared video microscopy. Pflügers Arch 423:511–518.

Svensson TH (2000) Dysfunctional brain dopamine systems induced by psychotomimetic NMDA-receptor antagonists and the effects of antipsychotic drugs. Brain Res Brain Res Rev 31:320–329.

Swanson LW (1982) The projections of the ventral tegmental area and adjacent regions: a combined fluorescent retrograde tracer and immunofluorescence study in the rat. Brain Res Bull 9:321–353.

Tan Y, Williams EA, Lancia AJ, Zahm DS (2000) On the altered expression of tyrosine hydroxylase and calbindin-D 28kD immunoreactivities and viability of neurons in the ventral tegmental area of Tsai following injections of 6-hydroxydopamine in the medial forebrain bundle in the rat. Brain Res 869:56–68.

Tsubokawa H, Mivva M, Kano M (1999) Elevation of intracellular Na^+ induced by hyperpolarization at the dendrites of pyramidal neurones of mouse hippocampus. J Physiol (Lond) 517:135–142.

Tzschentke TM (2001) Pharmacology and behavioral pharmacology of the mesocortical dopamine system. Prog Neurobiol 63:241–320.

Ulens C, Tytgat J (2001) Functional Heteromerization of HCN1 and HCN2 Pacemaker Channels. J Biol Chem 276:6069–6072.

Verhoeff NP (1999) Radiotracer imaging of dopaminergic transmission in neuropsychiatric disorders. Psychopharmacology (Berl) 147:217–249.

Waelti P, Dickinson A, Schultz W (2001) Dopamine responses comply with basic assumptions of formal learning theory. Nature 412:43–48.

Wainger BJ, DeGennaro M, Santoro B, Siegelbaum SA, Tibbs GR (2001) Molecular mechanism of cAMP modulation of HCN pacemaker channels. Nature 411:805–810.

Wilson CJ, Young SJ, Groves PM (1977) Statistical properties of neuronal spike trains in the substantia nigra: cell types and their interactions. Brain Res 136:243–260.

Wolfart J, Neuhoff H, Franz O, Roeper J (2001) Differential expression of the small-conductance, calcium activated potassium channel SK3 is critical for pacemaker control in dopaminergic midbrain neurons. J Neurosci 22:3443–3456.

Yu H, Wu J, Potapova I, Wymore RT, Holmes B, Zuckerman J, Pan Z, Wang H, Shi W, Robinson RB, El-Maghrabi MR, Benjamin W, Dixon J, McKinnon D, Cohen IS, Wymore R (2001) MinK-related peptide 1: a beta subunit for the HCN ion channel subunit family enhances expression and speeds activation. Circ Res 88:E84–E87.